

Scalable Expressiveness through Preprocessed Graph Perturbations

Danial Saber
danial.saber@ontariotechu.net
Ontario Tech University
Oshawa, Ontario, Canada

Amirali Salehi-Abari
abari@ontariotechu.ca
Ontario Tech University
Oshawa, Ontario, Canada

ABSTRACT

Graph Neural Networks (GNNs) have emerged as the predominant method for analyzing graph-structured data. However, canonical GNNs have limited expressive power and generalization capability, thus triggering the development of more expressive yet computationally intensive methods. One such approach is to create a series of perturbed versions of input graphs and then repeatedly conduct multiple message-passing operations on all variations during training. Despite their expressive power, this approach does not scale well on larger graphs. To address this scalability issue, we introduce *Scalable Expressiveness through Preprocessed Graph Perturbation (SE2P)*. This model offers a flexible, configurable balance between scalability and generalizability with four distinct configuration classes. At one extreme, the configuration prioritizes scalability through minimal learnable feature extraction and extensive pre-processing; at the other extreme, it enhances generalizability with more learnable feature extractions, though this increases scalability costs. We conduct extensive experiments on real-world datasets to evaluate the generalizability and scalability of SE2P variants compared to various state-of-the-art benchmarks. Our results indicate that, depending on the chosen SE2P configuration, the model can enhance generalizability compared to benchmarks while achieving significant speed improvements of up to 8-fold.

KEYWORDS

Graph Neural Networks, Scalability, Graph Perturbation

1 INTRODUCTION

Graph Neural Networks (GNNs) possess exceptional predictive capabilities on relational data (e.g., social networks, protein-protein interaction networks, etc.). Their applicability spans various domains, such as recommender systems [55], protein structure modeling [21], educational systems [45], and knowledge graph completion [1]. However, relational data’s complexity, scale, and dynamic nature pose substantial challenges to GNNs, emphasizing the importance of improving their generalization and computational efficiency.

Message-passing GNNs (MPNNs), a popular class of GNNs, facilitate the exchange of messages between nodes to integrate their local structural and feature information within a graph. Stacking multiple layers of message-passing allows the messages to be transmitted across longer distances in the graph, thus learning more global structural information. However, this approach increases computational complexity, particularly for larger graphs, and its generalization capabilities are limited by the 1-dimensional Weisfeiler-Lehman (1-WL) graph-isomorphism test [32].

Several approaches have been proposed to enhance the computational efficiency of message-passing GNNs. *Simplified graph neural*

networks (SGNNs) simplifies graph neural networks by removing their non-linearities between intermediate GNN layers, thus facilitating the preprocessing of message-passing for faster training [17, 19, 37, 54, 67]. Another acceleration approach involves sampling methods, where node neighborhoods are sampled during preprocessing [12, 36, 51, 63] or message-passing [10, 11, 23, 26, 59, 70] to reduce the number of messages during training or inference. The 1-WL expressivity constraint also extends to these scalability approaches for message-passing GNNs.

To go beyond 1-WL expressive power, many attempts are made. *Higher-order GNNs*, similar to the hierarchy in k -WL tests [34, 38], expand message-passing from individual nodes to node tuples, yielding richer representations. As an alternative approach, *Feature-augmented GNNs* integrate additional features like structural encodings [4, 7], geodesic distances [33, 53, 66], resistance distances [53], and positional encodings [16] for nodes or edges. Other approaches known as *Subgraph GNNs* focus on extracting multiple subgraphs for each node, using techniques such as node/edge labeling [27, 48, 61] or node/edge deletion [5, 27, 47, 49]. These techniques generate a variety of subgraph perturbations, enriching the graph’s representational diversity.

Despite their improved expressiveness, these approaches are less computationally efficient than the conventional GNNs. Higher-order GNNs require (at least) cubic computational complexity for message passing [65, 68]. Feature-augmented GNNs can struggle with scalability, as computing augmented features (e.g., structural encodings, resistance distance, shortest path distance, etc.) is computationally expensive for large graphs. Subgraph GNNs typically involve extracting or creating multiple large subgraphs from a larger graph and processing these with GNNs. Due to potential overlap among these subgraphs, their cumulative size can significantly expand, sometimes to hundreds of times the size of the original graph, rendering them impractical for large-scale graphs. For instance, DropGNN [47] generates multiple perturbations of the graph through random node removal and applies GNN on the perturbed graphs during training to enhance expressivity. However, scalability becomes a critical concern as the number of perturbations grows, confining the method’s applicability to smaller datasets.

Our approach. In our pursuit of formulating a flexible, scalable, and expressive model, we introduce *Scalable Expressiveness through Preprocessed Graph Perturbation (SE2P)*. Our approach offers four configuration classes, each offering a unique balance between scalability and generalizability. SE2P first creates multiple perturbations of the input graph through a perturbation policy (e.g., random node removal) and then diffuses nodal features through each perturbed graph. Unlike conventional message-passing GNNs, but similar to

SGNNs [17, 19, 37, 54, 67], the feature diffusion occurs once during preprocessing. Our SE2P differentiates from SGNNs by leveraging the expressive power offered by multiple perturbed graphs [5, 47]. The diffusions from each perturbation are *combined*, and nodal representations of all perturbations are *merged* to construct the final nodal profiles. Then, these profiles are subjected to a *pooling* operation for graph classification tasks to produce a vector representation of the entire input graph. A critical computational strength of our framework is its flexibility, allowing for the selection of aggregation functions (learnable or non-learnable), thus enabling scalable or expressive variations of many models. Depending on the selected configuration, our empirical results demonstrate significant speedup (up to 8 \times) compared to baselines while also improving the generalizability of expressive models such as DropGNN. Our experiments confirm that SE2P surpasses the generalization limitation of SGNNs (e.g., SGCNs, and SIGN) while offering comparable scalability. SE2P demonstrates flexibility in balancing expressiveness and scalability: The SE2P’s instance SE2P-C2 achieves 3-6 \times speed up with comparable generalizability to baselines, while another instance SE2P-C3 maintains baseline computational requirements and enhanced generalizability by up to 1.5%.

2 RELATED WORK

We review existing methods that enhance the scalability (i.e., computational efficiency) or expressiveness of Graph Neural Networks. We have identified key subdomains within these areas.

Simplification Methods (Scalability). To reduce the computational burden associated with multiple message-passing layers, one strategy [17, 19, 37, 54, 67] is to simplify GNN architectures by removing intermediate non-linearities, thus enabling feature propagation preprocessing across the graph. *Simplified Graph Convolutional Networks (SGCN)* [54] introduces a diffusion matrix by removing non-linearities from multi-layer Graph Convolutional Networks [28]. SIGN [19], GRAND [17], and NAFS [67] extend GCN to multiple diffusion matrices instead of a single one. Similarly, S3GRL [37] extends this technique to enrich the subgraph representations. However, many diffusion approaches (e.g., SGCN, SIGN, etc.) exhibit limited expressivity. Our SE2P framework leverages this feature diffusion approach while enhancing these models with graph perturbations to overcome their expressivity limitations.

Sampling Methods (Scalability). The sampling techniques are deployed to control the exponential growth of receptive fields across GNN layers for better scalability. *Node-based* sampling methods [11, 23, 59] samples fixed-size nodes’ neighborhoods for message-passing within mini-batches to reduce the nodes involved in the message-passing process. In contrast, *layer-based* sampling methods [10, 26, 70] targets the architectural level of GNNs by selectively sampling nodes for each layer. *Subgraph-based* sampling [12, 36, 51, 63] focuses on sampling subgraphs during preprocessing to handle large graphs on limited memory, and integrates these smaller, representative subgraphs into minibatches during training to update embeddings. Despite scalability, these sampling methods are limited to the 1-WL isomorphism test, necessitating enhancements in GNN expressivity.

Higher-order GNNs (Expressivity). Inspired by the higher-order WL tests [40], higher-order GNNs pass messages between node

tuples instead of individual nodes [3, 44]. To offset their high computational demands, localized and sparse higher-order aggregation methods have been developed [43], with the cost of reduced expressiveness [42].

Subgraph GNNs or Perturbed GNNs (Expressivity). An emerging body of research has focused on generating a bag of subgraphs (or perturbations) from an input graph and then applying GNNs on all subgraphs to get more expressive nodal representations. The primary distinction between these approaches is how subgraphs are generated or sampled. Some common techniques include node dropping [13, 17, 47], edge dropping [5, 49], node marking [48], and ego-networks [61, 65, 69]. The methods involving the removal of nodes or edges can also be viewed as regularization tools for GNNs, helping to reduce over-fitting [17, 49]. However, these methods often require a large number of perturbed graphs (or subgraphs) for each input graph, proportional to the graph size. For example, the number of perturbations that DropGNN [47] requires is set to be the average node degree (e.g., 75 perturbed graphs for each graph in the COLLAB dataset). Applying GNNs to this many perturbed graphs for a single input graph proves to be impractical, hindering scalability. Our approach shares some similarities with this body of research in generating perturbed graphs, albeit with a notable distinction: By once preprocessing diffused features of perturbed graphs, we ease the training computations, thus significantly improving scalability compared to DropGNN and other similar methods.

Feature augmented GNNs (Expressivity). Several studies have aimed to increase the expressiveness of GNNs by enriching or augmenting node features. Some examples of auxiliary/augmented node information include geodesic distances [33, 53, 66], resistance distances [53], subgraph-induced structural information [4, 7], and positional encodings [16]. Despite the potential of feature augmentation to improve expressiveness, they fall short in scalability, as computation of the auxiliary features (e.g., substructure counts, the shortest distance between pairs, etc.) is expensive for large graphs.

3 PRELIMINARY AND BACKGROUND

We consider an undirected graph $G = (V, E)$ with $|V| = n$ nodes, $|E| = m$ edges, and adjacency matrix $\mathbf{A} \in \mathbb{R}^{n \times n}$. Each node $i \in V$ possesses the d -dimensional feature vector $\mathbf{x}_i \in \mathbb{R}^d$, which can be viewed as the i -th row of $n \times d$ feature matrix \mathbf{X} .

3.1 Graph Prediction Task

Graph classification or regression involves predicting a label (e.g., carcinogenicity classification [52]) or a property (e.g., molecule solubility level [22]) for an entire graph based on its structure and associated features (e.g., node or edge features).¹ Specifically, the task is formulated as a supervised learning problem, aiming to learn a mapping function $f : \mathcal{G} \rightarrow \mathcal{Y}$, given a labeled dataset $D = \{(G_i, y_i)\}$, where \mathcal{G} is input space, and \mathcal{Y} is class label space (or real for regression), G_i is input graph sample, and y_i is an expected label (or property). Graph Neural Networks have demonstrated significant success in effectively addressing the challenges of graph classification or regression tasks [24].

¹Although our proposed models readily apply to other downstream tasks on graphs such as node classifications or link predictions, we focus on graph-level prediction tasks for conciseness.

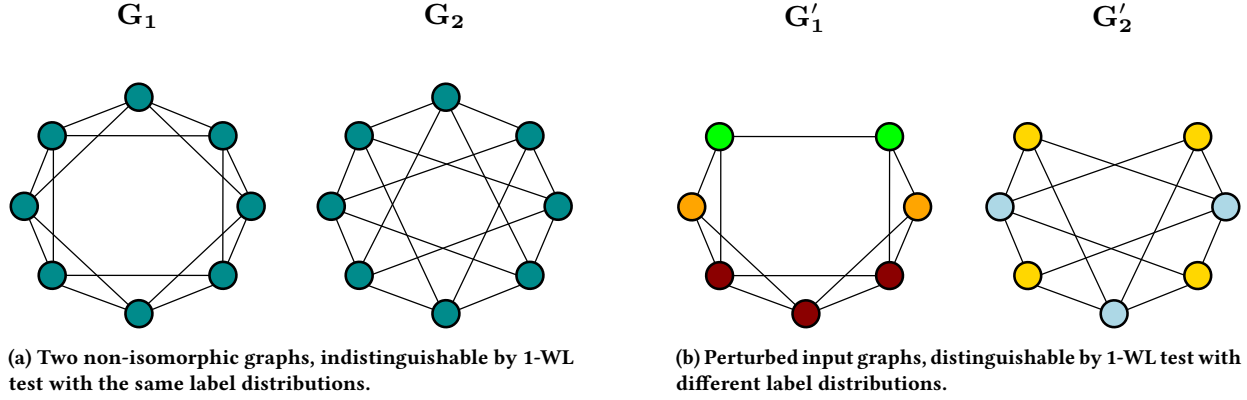


Figure 1: 1-WL graph isomorphism test (a) fails to distinguish between two non-isomorphic graphs G_1 and G_2 , but (b) successfully detect their perturbation (through node removal) G'_1 and G'_2 .

3.2 Graph Neural Networks

In message-passing *Graph Neural Networks* (GNNs), each node’s representation \mathbf{h}_i is iteratively *updated* and refined through the *aggregation* of messages received from its neighbor’s representations.² In GNNs, the node i ’s representation at step (or layer) l is updated by:

$$\mathbf{h}_i^{(l)} = \text{UPDATE} \left(\mathbf{h}_i^{(l-1)}, \mathbf{m}_{N(i)}^{(l-1)} \right) \quad (1)$$

where $\mathbf{m}_{N(i)}^{(l-1)}$ is the message aggregated from i ’s neighborhood $N(i)$:

$$\mathbf{m}_{N(i)}^{(l-1)} = \text{AGGREGATE} \left(\left\{ \mathbf{h}_j^{(l-1)} \mid j \in N(i) \right\} \right). \quad (2)$$

GNNs usually differ from one another in how their AGGREGATE and UPDATE functions are defined. For example, *graph convolutional networks* (GCN) [28] employ a degree-normalized weighted mean as the AGGREGATE function:

$$\mathbf{m}_{N(i)}^{(l-1)} = \sum_{j \in N(i)} \frac{\mathbf{h}_j^{(l-1)}}{\sqrt{|N(i)||N(j)|}}, \quad (3)$$

followed by a simple update function of:

$$\mathbf{h}_i^{(l)} = \sigma \left(\mathbf{W}^{(l)} \left(\frac{\mathbf{h}_i^{(l-1)}}{|N(i)|} + \mathbf{m}_{N(i)}^{(l-1)} \right) \right), \quad (4)$$

where σ is a non-linearity function (e.g., ReLU), and $\mathbf{W}^{(l)}$ is the l^{th} layer’s learnable weight matrix. In GNNs, for each node $i \in V$, the initial node representation at step 0 is usually set to their original node features: $\mathbf{h}_i^{(0)} = \mathbf{x}_i$. After L message-passing iterations, the node i ’s representation \mathbf{z}_i is the output of layer L , i.e., $\mathbf{z}_i = \mathbf{h}_i^{(L)}$, or a combination of all L layers’ outputs $\mathbf{z}_i = \text{COMBINE}(\mathbf{h}_i^{(1)}, \dots, \mathbf{h}_i^{(L)})$ [57]. One can view all learned node’s representations in the form $n \times d'$ matrix \mathbf{Z} , where d' is the hidden dimensionality. All nodes’ final representations are then aggregated to form a graph (vector) representation:

$$\mathbf{z}_G = \text{POOL} (\{ \mathbf{z}_i \mid i \in G \}), \quad (5)$$

²We use the abbreviation GNNs interchangeably with MPNNs, although MPNNs are a subclass of GNNs.

where the POOL function can be non-adaptive (e.g., element-wise mean or max) or adaptive (e.g., top-k pooling [20, 30], set transformer [8], or MLP [8]). The class probabilities are then computed by passing \mathbf{z}_G through a non-linear learnable transformation (e.g., MLP).

Despite the success of GNNs, their expressive power is limited and upper bounded by the 1-WL test [44, 56]. This limitation necessitates the development of new approaches with enhanced expressiveness.

3.3 Perturbed Graph Neural Networks

To overcome 1-WL expressivity limitation of canonical GNNs [44, 56], *Perturbed GNNs* (e.g., DropGNN [47]) applies a shared GNN on R different perturbations of the input graph (during both training and testing). For each perturbation (A_r, X_r) , some graph structure (e.g., nodes or edges) is randomly changed. For example, DropGNN randomly drops out some nodes for each perturbation, allowing a shared L -layer GNN to operate on a slightly perturbed version of the input graph to generate perturbed node representations $\mathbf{Z}_r = \text{GNN}(A_r, X_r)$. These perturbed embeddings are then merged into final node embeddings using an aggregator function:

$$\mathbf{Z} = \text{MERGE} (\mathbf{Z}_1, \dots, \mathbf{Z}_R), \quad (6)$$

where MERGE can be an element-wise mean operator. Through multiple perturbations, the model observes slightly perturbed variants of the same L -hop neighborhood around any node. Thus, even if the non-isomorphic neighborhoods are indistinguishable by the standard GNNs (or 1-WL), their randomly modified variants are more likely to be distinguishable, yielding higher expressive power. For example, in Figure 1a, there are two non-isomorphic graphs which differ by the presence or absence of 3-length cycles (left graph vs right graph). The 1-WL algorithm cannot distinguish these two graphs as non-isomorphic. However, after a slight perturbation by removing a node (see Figure 1b), the 1-WL test successfully identifies them as non-isomorphic.

For graph classification, the node representations \mathbf{Z} in Equation 6 can be aggregated by a POOL function into a graph-level representation \mathbf{z}_G . However, Perturbed GNNs (e.g., DropGNN) face major scalability issues as the number of perturbations increases,

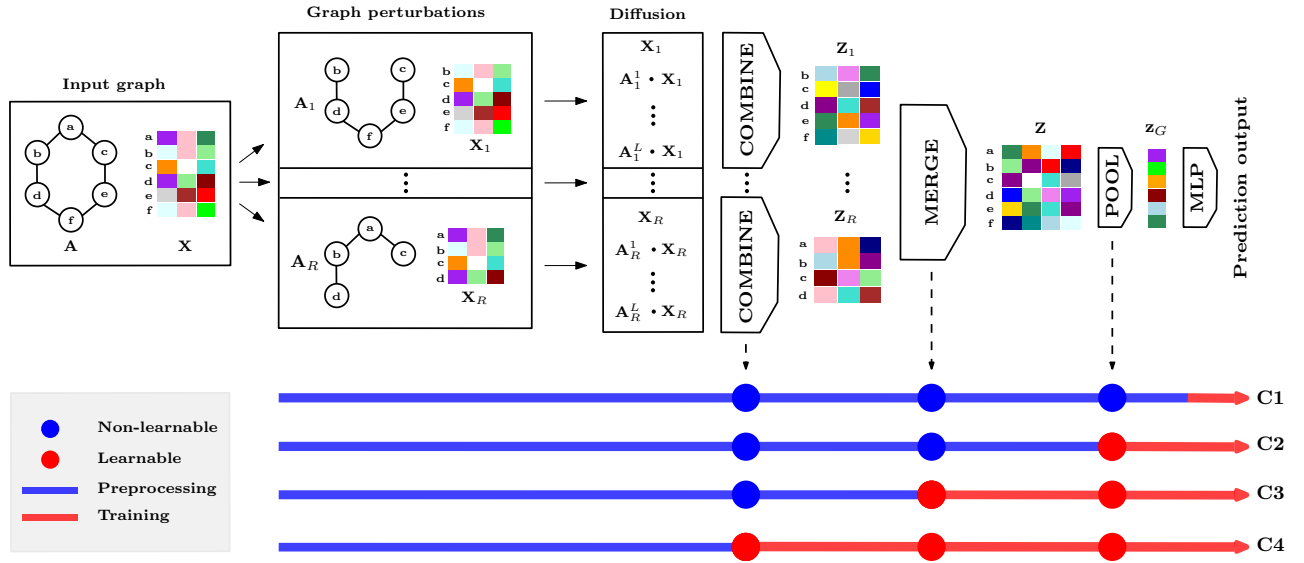


Figure 2: The *SE2P* framework first generates R perturbations of the input graph, where each perturbation involves randomly removing some nodes, thereby resulting in new adjacency and feature matrices (A_r, X_r) . Next, node features are diffused for each perturbation by a set of diffusion matrices: the perturbed adjacency matrix powers. Then, the *COMBINE* function combines these diffused features for each perturbed graph to produce feature matrices Z_r . All these matrices then undergo the *MERGE* function to generate a single nodal representation matrix Z for the input graph. Focusing on the graph-level task, we then apply *POOL* to yield a graph (vector) representation z_G and further achieve the predicted output through a non-linear transformation by *MLP*. The functions *COMBINE*, *MERGE*, and *POOL* can be either non-learnable (blue circle) or learnable (red circle). This flexibility allows us to choose between different configuration classes (C1, C2, C3, and C4) to balance scalability, achieved by including more preprocessing steps (blue line), and expressivity, achieved by having more learnable components and a longer training phase (red line).

hindering their effectiveness on large datasets with high average node degrees.

3.4 Simplified Diffusion-Based Models

A practical approach to enhance the scalability of GNNs is simplifying their architectures by eliminating their intermediate non-linearities [17, 19, 37, 54, 67]. This simplification technique allows for the precomputation of feature propagation and further acceleration. For instance, SGCN [54] removes intermediate non-linearities in an L -layer GCN, to predict node class labels Y using $Y = \sigma(A^L X W)$, where σ is a non-linear function, and W is a learnable weight matrix. The diffusion term $A^L X$ can be precomputed once before training. Extending upon SGCN, SIGN [19] considers a set of diffusion matrices $\{S^{(i)}\}$ (rather than just one diffusion matrix) to apply to the feature matrix X :

$$Z = \sigma \left(\bigoplus_i S^{(i)} X W_i \right), \quad (7)$$

where W_i is a learnable weight matrix associated with the diffusion matrix $S^{(i)}$. Like SGCN, the terms $S^{(i)} X$ can be precomputed before training to speed up computation. The diffusion terms in our model share some similarities to SIGN. However, unlike our method, the expressivity of SGCN and SIGN is bounded by the 1-WL, as they were proposed to make the traditional GNNs more scalable.

4 SE2P

Inspired by the expressive power of methods relying on generating perturbations (e.g., DropGNN [47]), yet motivated to address the scalability limitations, we propose *Scalable Expressiveness through Preprocessed Graph Perturbations (SE2P)*. In *SE2P*, we first generate different perturbations of the input graph (e.g., through random node dropout) to improve expressiveness. The scalability is offered by once precomputing feature diffusions over perturbed graphs and eliminating the need for message-passing during training.

As illustrated in Fig. 2, *SE2P* generates a set of R graph perturbations $\{(A_r, X_r)\}$ for graph G with adjacency matrix A and feature matrix X . Although *SE2P* accommodates any perturbation kind (e.g., node removal, subgraph sampling, etc.), we here consider random nodal removal as a perturbation. In each perturbation (A_r, X_r) , any node of the original graph G is removed with probability p .³ Each perturbed adjacency matrix A_r is normalized by $\hat{A}_r = D_r^{-\frac{1}{2}} A_r D_r^{-\frac{1}{2}}$, where D_r is the diagonal matrix of A_r .⁴ To emulate the message-passing of GNNs on perturbed graphs, we apply feature diffusion

³A common implementation trick for the removal of a node is to set its corresponding row and column in the adjacency matrix to all zeros. This trick allows the dimensionality of the adjacency matrices of all perturbed graphs to remain the same, thus easing aggregations downstream in pipelines. When this trick is used, the feature matrix for perturbation graphs is kept as the original one.

⁴While adding self-loops to the adjacency matrix could offer certain benefits (e.g., over-fitting prevention), we deliberately avoid them in our approach. Our decision is backed up by the understanding that self-loops restrict generalizability by making the self or other's information indistinguishable [24].

by $\hat{A}_r X_r$. Similarly, the message passing of an L -layer GNN can be emulated by $\hat{A}_r^L X_r$, which can be once precomputed before the training for each perturbed graph as a preprocessing step. For each perturbed graph, to have a more expressive node representation, we emulate the jumping knowledge [56] by

$$Z_r = \text{COMBINE}(X, \hat{A}_r^1 X_r, \dots, \hat{A}_r^L X_r), \quad (8)$$

where the COMBINE function combines all the virtual L layer’s output with the original feature matrix into the node embedding matrix of the perturbed graph. The examples of COMBINE can be simple readout-type operators (e.g., column-wise vector concatenation, etc.) or learnable adaptive aggregation mechanisms (e.g., LSTM or DeepSet). When the simple non-learnable operator is deployed, we compute Z_r through preprocessing steps for more speedup.

The next step is to aggregate node representations of perturbed graphs $\{Z_r\}$ to a single nodal representation matrix Z :

$$Z = \text{MERGE}(Z_1, \dots, Z_R), \quad (9)$$

where several options exist for MERGE ranging from non-learnable aggregation methods (e.g., element-wise mean) to learnable set aggregations (e.g., DeepSet [62]). While non-learnable aggregation methods, such as averaging, provide simplicity and computational efficiency, they may override and blend information across perturbed graphs, possibly leading to the loss or dilution of discriminative information. However, all computations up to this point can occur during the preprocessing phase, provided that aggregations in Eqs. 8 and 9 are non-learnable. This preprocessing offers a considerable speedup, as it emulates the message-passing of a multi-layer GNN on multiple perturbed graphs through a one-time preprocessing step rather than iterative computations during training. When more expressiveness is desired over scalability, one can employ learnable aggregation over perturbed graphs.

For graph prediction tasks (i.e., graph classification and regressions), we then apply a POOL function to aggregate nodes’ final representations into a graph (vector) representation:

$$z_G = \text{POOL}(Z), \quad (10)$$

where z_G is the graph representation and the POOL function can be non-learnable (e.g., element-wise sum) or a learnable graph pooling method. Non-learnable functions can speed up computation (specifically if they facilitate precomputation); However, they come at the cost of not introducing any non-linearity to the model to output graph representation, thus reducing the model’s expressive power to some extent. If higher expressiveness is desired, given some computational budget, one might consider various learnable graph pooling methods such as hierarchical or top-k pooling [9, 20, 29, 60], global soft attention layer [35], set-transformer [31], or even MLP combined non-learnable aggregators (e.g., sum or mean). After the pooling operation, we apply a learnable non-linear function ω to get the class probabilities y from graph representation z_G :

$$y = \omega(z_G). \quad (11)$$

How does SE2P trade-off scalability and expressivity? The SE2P’s aggregation functions COMBINE, MERGE, and POOL offer a balance between scalability and expressivity. We can configure each to belong to either learnable or non-learnable aggregator classes. Thus, we specify four practical *configuration classes* within SE2P for

Table 1: The experimented non-learnable or learnable aggregation functions of the SE2P configurations.

Configuration	COMBINE	MERGE	POOL
SE2P-C1	Concat	Mean	Sum
SE2P-C2	Concat	Mean	MLP + Sum
SE2P-C3	Concat	DeepSet	MLP + Sum
SE2P-C4	DeepSet	DeepSet	MLP + Sum

balancing scalability vs expressiveness. Each configuration class is identified by which aggregator is learnable or not.⁵ All functions can be configured to be non-learnable (e.g., element-wise mean, sum, or max) for maximum scalability (see configuration class C1 in Fig. 2). This offers the highest scalability as all the computations up to obtaining the graph (vector) representation can be once precomputed before training. By exploiting a learnable function for POOL while keeping COMBINE and MERGE non-learnable, we can improve the expressivity of the model before generating the graph representation (see configuration class C2 in Fig. 2). In this class, one can still preprocess the perturbed graphs, their diffusion, COMBINE, and MERGE for improved efficiency. Going one step further to enhance the expressivity, we can select MERGE as learnable in addition to POOL (see configuration class C3 in Fig. 2). In this class, the diffused matrices of the graph perturbations will be merged in the training stage. Given the desired computational resources, one can select learnable functions for all the aggregation functions. This configuration will be the least scalable configuration class (C4 in Fig. 2). Moving from C1 to C4 increases expressiveness but reduces scalability, as it allows less preprocessing to ease training’s computational burden.

Our experimented configurations for SE2P. We have implemented and studied four instances of SE2P, covering all four configuration classes, with specific COMBINE, MERGE, and POOL functions. SE2P-C1 uses column-wise vector concatenation for COMBINE, element-wise mean for MERGE, and element-wise sum pooling for POOL. With all non-learnable aggregation functions, all operations up to generating the graph representations are precomputed for maximum scalability. SE2P-C2 replaces the sum pooling of SE2P-C1 with a learnable POOL function, which consists of an MLP followed by element-wise sum pooling. SE2P-C3 is the same as SE2P-C2 except for leveraging DeepSet as a learnable MERGE function (rather than non-learnable element-wise mean in SE2P-C2). The least scalable configuration SE2P-C4 replaces the non-learnable COMBINE of SE2P-C3 to DeepSet, making all aggregator functions learnable for maximum expressivity. Table 1 summarizes the selected aggregation functions of the configurations.

4.1 Runtime Analysis

We investigate the (amortized) preprocessing and training time complexity per graph instance for DropGNN and our examined SE2P variants (see Table 2 for summary). For simplicity of representations, through our analyses, we assume that both input data

⁵ Given three aggregation functions, and two choices of learnability for each, one can theoretically identify 8 potential classes. But, not all those classes would be beneficial for scalability if a learnable aggregator comes before a non-learnable one.

dimensionality d and hidden representation dimensionality h have the same order of dimensionality $O(d)$.

For DropGNN, the preprocessing time is $O(1)$. For its training, the R perturbations are generated in $O(Rn)$ by creating a dropout mask to zero out the connection of removed nodes, assuming that the graph is stored in a sparse matrix. For inference, the model applies L layers of graph convolution and a two-layer MLP on each perturbation, which runs in $O(RL(nd^2 + md) + nd^2)$ time, assuming d is the feature dimension and proportional to the hidden dimensionality of both graph convolutions and MLP, and m is number of edges. The inference time complexity of DropGNN is $O(Rn + RL(nd^2 + md) + d^2) = O(RL(nd^2 + md))$.

Table 2: Running time complexities of DropGNN and SE2P configurations. R denotes the number of perturbations, L is the number of virtual layers of the diffusion step, n is the number of nodes, m is the number of edges, and d is the feature dimensionality or the hidden dimensionality.

Model	Preprocessing	Inference
DropGNN	$O(1)$	$O(RL(nd^2 + md))$
SE2P-C1	$O(RLmd)$	$O(d^2)$
SE2P-C2	$O(RLmd)$	$O(nd^2)$
SE2P-C3	$O(RLmd)$	$O(Rnd^2)$
SE2P-C4	$O(RLmd)$	$O(RLnd^2)$

The preprocessing time for all SE2P variants is $O(RLmd)$. The preprocessing in SE2P-C4 involves two parts: (i) creating R node-removal perturbations in $O(Rn)$ time; (ii) diffusion of features over RL sparse adjacency matrices of graphs with $O(m)$ edges in $O(RLmd)$ time. Note that $O(Rn + RLmd) = O(RLmd)$. The SE2P-C3 has an extra concatenation in $O(RLnd)$ time, dominated by $O(RLmd)$, thus again the total preprocessing time of $O(RLmd)$. The MERGE function of Mean in both SE2P-C1 and SE2P-C2 has a running time of $O(RLnd)$, and Sum for POOL in SE2P-C1 has a running time of $O(Rnd)$; all are dominated by $O(RLmd)$, rendering the total running time for SE2P-C1 and SE2P-C2 again $O(RLmd)$.⁶

For inference, SE2P-C1 only applies the MLP transformation to the graph representation for graph classification, resulting in a time complexity of $O(d^2)$. SE2P-C2 adds another learnable component in the POOL function (MLP + SUM), with time complexity of $O(nd^2)$. Thus, the SE2P-C2 infer in $O(nd^2 + d^2) = O(nd^2)$ time. Compared to SE2P-C2, SE2P-C3 has an additional learnable DeepSet for MERGE to combine perturbations. This DeepSet runs in $O(Rnd^2 + nd^2) = O(Rnd^2)$, dominating other running times of POOL and final transformation, thus making SE2P-C3 running time $O(Rnd^2)$. SE2P-C4 has an additional DeepSet as COMBINE for aggregating the L virtual layer’s representations in each perturbation, which runs in $O(RLnd^2)$. As this dominates other components’ running time asymptotically, the time complexity of SE2P-C4 is $O(RLnd^2)$.

⁶To achieve faster and more scalable preprocessing implementations for SE2P, one can parallelize sparse matrix multiplications using frameworks for distributed computing (e.g., Spark, etc.), which is not explored in this work.

5 EXPERIMENTS

Our experiments aim to empirically validate the scalability (e.g., runtime, memory requirements, etc.) and generalizability of our SE2P models against various benchmarks on graph prediction tasks.

Datasets. For graph classification tasks, we experiment with six datasets from the TUDataset collection [41]: three *bioinformatics datasets* of MUTAG [14], PROTEINS [6, 15], and PTC-MR [52]; and three *social network datasets* of IMDB-B [58], IMDB-M [58], and COLLAB [58]. These datasets have been the subject of study for other prominent graph classification methods [5, 18, 47, 56, 69]. The bioinformatics datasets contain categorical nodal features, while the social network datasets do not have any nodal features. As with others [5, 47, 56], we encode node degrees as node features for datasets without nodal features. For TU datasets, we use the same dataset splitting deployed by other related studies [5, 47, 56, 69], which is 10-fold cross-validation. We also test our model on the OGBG-MOLHIV and OGBG-MOLTOX datasets from Open Graph Benchmark (OGB) [25] using their provided scaffold splits. Their provided splits have been widely used among other works evaluating OGB benchmarks [5, 69]. We provide the statistics of all datasets in Table 3.

Baselines. For graph classification on TU datasets, we assess and compare our model with several state-of-the-art baselines: the WL subtree kernel [50], Diffusion convolutional neural networks (DCNN) [2], Deep Graph CNN (DGCNN) [64], PATCHY-SAN [46], IGN [39], GCN [28], GIN [56], DropGIN [47], and DropGCN.⁷ On open Graph Benchmark datasets, we compare our proposed models against GCN, GIN, DropGCN, and DropGIN.

Experimental setup. For a fair comparison between DropGNN [47] and SE2P variants, we adopt the recommended hyperparameters for DropGNN by setting the probability of dropping node $p = \frac{2}{1+\gamma}$ and the number of perturbations $R = \lfloor \gamma \rfloor$, where γ is the average node degree in the dataset.⁸ The number of (virtual) layers L is set to 2 or 3 for each dataset.⁹ For TU benchmark evaluations, we present the accuracies of the WL subtree kernel, DCNN, DGCNN, PATCHY-SAN, and IGN, as reported in their original papers.¹⁰ Under this experimental setup, we also reproduced the results for GCN [28], GIN [56], DropGIN [47], and DropGCN. We grid-searched the hyperparameters for these baselines on the recommended search spaces [47]. For the SE2P variants, we performed a hyperparameter search for each dataset using a cascading approach from SE2P-C1 to SE2P-C4: Once hyperparameters are determined for a component of a model (e.g., final MLP transformation component in SE2P-C1), they are kept the same across all subsequent configurations (e.g., SE2P-C2 to SE2P-C4). A subsequent hyperparameter search is then conducted on the immediate subsequent variant (e.g., SE2P-C2) while focusing solely on its introduced hyperparameters (e.g., hyperparameters for the POOL function in SE2P-C2). Then, the tuned

⁷Our introduced DropGCN has replaced GIN layers with GCN layers in DropGIN.

⁸Theoretical analysis for choosing the number of perturbations have been provided in DropGNN [47].

⁹Motivated by the observation that a lower L for denser graphs yield better generalization [67], we have set $L=2$ if the average degree less than 10; otherwise $L=3$.

¹⁰Similarly, many other relevant studies [5, 47, 56], which share the same experimental setup as ours, have borrowed these results from their original papers.

Table 3: Statistics of all the datasets used in our experiments.

Dataset	Task	#Graphs	Avg. Nodes	Avg. Deg.	#Classes	Feat. Type
MUTAG	Classify mutagenicity of compounds	188	17.93	3.01	2	Original
PROTEINS	Classify enzyme & non-enzyme	1109	39.06	5.78	2	Original
PTC-MR	Classify chemical compounds	344	14.29	3.18	2	Original
IMDB-B	Classify movie genre	996	19.77	18.69	2	Encoded
IMDB-M	Classify movie genre	1498	12.9	11.91	3	Encoded
COLLAB	Classify researcher fields	5000	74.49	73.49	3	Encoded
OGBG-MOLTOX21	Classify qualitative toxicity measurements	7831	19	3.27	12	Original
OGBG-MOLHIV	Classify HIV virus replication	41127	25.5	3.38	2	Original

Table 4: Average validation accuracy (%), TU datasets. The best result is in bold. In parenthesis: the ranks of our model against baselines (1st, 2nd, and 3rd are colored), and comparison to DropGNNs (●=better, ●=comparable with difference < 0.2, and ●=worse). OOM denotes out of memory.

Model / Dataset	MUTAG	PROTEINS	PTC-MR	IMDB-B	IMDB-M	COLLAB
WL subtree	90.4 ± 5.7	75.0 ± 3.1	59.9 ± 4.3	73.8 ± 3.9	50.9 ± 3.8	78.9 ± 1.9
DCNN	67.0 ± 2.1	61.3 ± 1.6	56.6 ± 1.2	49.1 ± 1.4	33.5 ± 1.4	52.1 ± 2.7
DGCNN	85.8 ± 1.7	75.5 ± 0.9	58.6 ± 2.5	70.0 ± 0.9	47.8 ± 0.9	73.7 ± 0.4
PATCHYSAN	89.0 ± 4.4	75.0 ± 2.5	62.3 ± 5.7	71.0 ± 2.3	45.2 ± 2.8	72.6 ± 2.2
IGN	83.9 ± 13.0	76.6 ± 5.5	58.5 ± 6.9	72.0 ± 5.5	48.7 ± 3.4	78.3 ± 2.5
GIN	88.8 ± 5.7	75.4 ± 5.0	63.9 ± 8.3	75.5 ± 4.0	51.5 ± 4.0	82.2 ± 2.1
GCN	85.5 ± 9.4	75.9 ± 5.5	64.2 ± 9.7	75.7 ± 3.6	52.0 ± 4.1	82.6 ± 2.2
DropGIN	89.1 ± 9.2	76.1 ± 5.1	65.2 ± 9.8	75.2 ± 3.1	52.3 ± 3.8	OOM ^a
DropGCN	87.1 ± 9.7	76.1 ± 5.8	64.5 ± 9.1	75.3 ± 3.3	52.1 ± 3.3	OOM ^a
SE2P-C1	87.8 ± 6.9 (5, ●)	74.7 ± 5.7 (9, ●)	64.5 ± 8.0 (2, ●)	74.6 ± 3.7 (5, ●)	52.1 ± 2.8 (2, ●)	79.8 ± 1.5 (3, ●)
SE2P-C2	89.4 ± 7.4 (2, ●)	77.6 ± 6.3 (1, ●)	65.1 ± 7.3 (2, ●)	75.2 ± 2.9 (3, ●)	52.3 ± 2.3 (1, ●)	83.3 ± 2.1 (1, ●)
SE2P-C3	89.5 ± 6.6 (2, ●)	77.6 ± 5.0 (1, ●)	66.2 ± 6.8 (1, ●)	75.9 ± 3.4 (1, ●)	52.9 ± 3.5 (1, ●)	83.5 ± 1.7 (1, ●)
SE2P-C4	89.7 ± 7.5 (2, ●)	76.8 ± 4.7 (1, ●)	66.1 ± 8.8 (1, ●)	75.7 ± 4.8 (2, ●)	52.4 ± 2.4 (1, ●)	82.8 ± 2.1 (1, ●)

^a We encountered out-of-memory issues with DropGNN on the COLLAB dataset due to the large number of graphs and perturbations, but reducing the batch size (e.g., from 32 to 6 in DropGCN on our server) allows these models to run. However, this resulted in suboptimal performance, leading us to report OOM results to highlight computational bottlenecks rather than expressiveness concerns.

hyperparameters are again fixed and copied to all subsequent variants (e.g., SE2P-C3 and SE2P-C4). The cascading process continues until all hyperparameters of the last variant are tuned.¹¹

Similar to *Xu et al.* [56], our experimental setup involves a 10-fold cross-validation. For each fold, we optimized a model with Adam for 350 epochs, and an initial learning rate of 0.01 decayed by a factor of 0.5 every 50 epochs. In this setup, datasets are split into training and validation sets (without a separate test set), and the reported results are on the validation accuracy. We obtain 10 validation curves corresponding to the 10 folds, calculate the average validation curve across all folds, and then select an epoch that achieves the highest averaged validation accuracy. We also compute standard deviation over the 10 folds at the selected epoch. For the OGB benchmark, we employed the same hyperparameter tuning approach as we did

¹¹We note that our cascading hyperparameter tuning procedure is suboptimal, but this process considerably speeds up our hyperparameter search by limiting the exponential growth of search space and running the (sub)optimal hyperparameters of previous models.

for the TU benchmark, and then followed the evaluation procedure proposed in [25]: we ran each experiment with 10 different random seeds, optimized using Adam for 100 epochs. We obtained the element-wise mean of the validation curves of all the seeds and determined the test accuracies (and their average) corresponding to the best validation accuracy.¹²

Results and Discussions. We present the validation accuracy results on TU datasets in Table 4. In all datasets except MUTAG, SE2P-C3 outperforms other SE2P configurations and baselines, and improves the generalizability over all baselines ranging from 0.6% (in IMDB-M) to 1.5% (in PROTEINS). SE2P-C2 and SE2P-C4 also show competitive performance, securing the top three-ranked methods among all baselines for all datasets. For instance, SE2P-C4 improves or shows comparable results to all baselines in all datasets except MUTAG, where the WL subtree model performed best. Our least

¹²The code is available at <https://github.com/Danial-sb/SE2P>. All experiments were conducted on a server with 40 CPU cores, 377 GB RAM, and 11 GB GTX 1080 Ti GPU.

Table 5: Runtime Analysis over TU datasets. The training time is the average time per epoch (over 350 epochs), and the runtime is the processing time and the training time. SE2Ps are color-coded by faster, comparable, and slower than the baselines. The maximum and minimum speedup corresponds to the ratio of time taken by the slowest and the fastest baselines compared to our model. All results are reported in seconds.

Model	MUTAG			PROTEINS			PTC-MR			IMDB-B			IMDB-M			COLLAB		
	Prep.	Train	Run	Prep.	Train	Run	Prep.	Train	Run	Prep.	Train	Run	Prep.	Train	Run	Prep.	Train	Run
GIN	–	0.71	248	–	0.74	259	–	1.52	532	–	0.71	248	–	0.72	252	–	3.87	1354
GCN	–	0.76	266	–	0.71	248	–	0.64	224	–	0.77	269	–	0.73	255	–	2.62	918
DropGIN	–	0.82	287	–	0.86	301	–	1.74	609	–	1.05	367	–	0.94	329	–	OOM	OOM
DropGCN	–	1.04	364	–	0.94	329	–	0.86	303	–	0.99	348	–	1.19	418	–	OOM	OOM
SE2P-C1	0.5	0.26	92	8.7	0.27	103	1.8	0.22	79	3.8	0.22	81	4.0	0.23	84	230.3	0.26	321
Max speedup	–	4.00	3.96	–	3.48	3.19	–	7.90	7.70	–	4.77	4.53	–	5.17	4.97	–	14.88	4.21
Min speedup	–	2.73	2.69	–	2.62	2.40	–	2.90	2.83	–	3.22	3.06	–	3.13	3.00	–	10.07	2.85
SE2P-C2	0.5	0.42	148	8.7	0.41	152	1.7	0.28	101	3.8	0.38	137	4.0	0.37	133	224.2	0.72	476
Max speedup	–	2.47	2.45	–	2.29	2.16	–	6.21	6.02	–	2.76	2.67	–	3.13	3.14	–	5.37	2.84
Min speedup	–	1.69	1.67	–	1.73	1.63	–	2.28	2.21	–	1.86	1.81	–	1.89	1.89	–	3.63	1.92
SE2P-C3	0.5	1.19	417	8.5	1.34	477	1.6	0.70	247	2.9	0.85	300	3.1	0.82	291	220.2	20.06	7241
Max speedup	–	0.87	0.87	–	0.70	0.68	–	2.48	2.46	–	1.19	1.22	–	1.45	1.43	–	0.19	0.18
Min speedup	–	0.59	0.59	–	0.52	0.51	–	0.91	0.90	–	0.83	0.82	–	0.87	0.86	–	0.12	0.12
SE2P-C4	0.5	5.22	1827	8.5	7.06	2479	1.4	3.58	1254	2.9	3.90	1368	3.0	2.61	918	214.7	42.86	15215
Max speedup	–	0.19	0.19	–	0.13	0.13	–	0.48	0.48	–	0.26	0.26	–	0.45	0.45	–	0.09	0.08
Min speedup	–	0.13	0.13	–	0.10	0.09	–	0.17	0.17	–	0.18	0.18	–	0.27	0.27	–	0.06	0.05

Table 6: Average ROC-AUC (%) over 10 runs on OGB datasets. The best is in bold. The preprocessing time, training time per epoch, and the total runtime are provided in seconds. Color-coding is faster, comparable, and slower than any of baselines.

Model	OGBG-MOLHIV					OGBG-MOLTOX21				
	Validation	Test	Prep.	Time/epoch	Run	Validation	Test	Prep.	Time/epoch	Run
GIN	78.1 ± 2.0	74.0 ± 1.9	–	3.54	354	75.6 ± 1.1	72.7 ± 1.7	–	1.56	156
GCN	78.6 ± 2.4	74.1 ± 1.9	–	3.56	356	76.0 ± 0.8	72.2 ± 1.1	–	1.71	171
DropGIN	OOM	OOM	–	–	–	75.7 ± 0.7	73.6 ± 1.0	–	2.33	233
DropGCN	OOM	OOM	–	–	–	76.2 ± 0.7	72.1 ± 1.1	–	2.52	252
SE2P-C1	73.1 ± 2.0	71.4 ± 1.3	170.5	1.79	349	72.6 ± 0.4	71.6 ± 0.5	22.6	0.59	81
SE2P-C2	77.1 ± 0.9	74.0 ± 1.3	169.7	2.23	393	76.1 ± 0.8	72.9 ± 0.6	22.5	0.87	109
SE2P-C3	76.3 ± 2.2	74.5 ± 2.6	171.6	11.21	1292	76.7 ± 0.9	73.5 ± 1.0	22.6	2.46	268
SE2P-C4	OOM	OOM	173.1	–	–	77.0 ± 1.3	74.1 ± 1.0	22.6	11.36	1158

expressive SE2P-C1 model performs suboptimally on three datasets of MUTAG, PROTEINS, and IMDB-B, but is relatively competitive in other datasets (e.g., PTC-MR, IMDB-M, COLLAB) by being ranked among the top three of baselines. The poor performance in those three datasets might be due to the lack of non-linearity before obtaining the graph representation and complexity of those datasets. Notably, for most datasets, models involving perturbation generation (SE2P, DropGCN, and DropGIN) outperform most baselines that do not utilize graph perturbation (e.g., GCN, IG). This result suggests that graph perturbations are not only a theoretically-founded method for going above 1-WL expressiveness, but are a

simple yet effective method for improving generalization. Comparing our SE2P models with DropGNN, which benefits from the power of graph perturbations, our configurations (except for SE2P-C1) always show comparable or improved generalizability. This generalization improvement is also complemented by handling the scalability issues of DropGNN (e.g., OOM in COLLAB and longer training times for other datasets).

However, graph perturbations in DropGNNs are not computationally efficient as for the largest dataset COLLAB, memory limitations prevented the assessment of these models on this dataset, as it requires the generation of nearly a hundred perturbations for each

Table 7: Ablation study comparing the impact of removing perturbations and the MERGE function (SIGN), removing perturbations and COMBINE and MERGE functions (SGCN) versus SE2P-C2 on TU datasets. The preprocessing time (Pre), training time per epoch (Train), and the total runtime (Run) are provided in seconds. Reported results are in terms of graph classification validation accuracy (Val). The best is highlighted in bold.

Model	MUTAG				PROTEINS			
	Pre	Train	Run	Val	Pre	Train	Run	Val
SGCN	0.1	0.41	144	87.7 ± 8.9	0.5	0.41	143	76.2 ± 5.3
SIGN	0.1	0.43	150	87.2 ± 9.6	0.7	0.41	143	76.4 ± 5.7
SE2P-C2	0.5	0.42	148	89.4 ± 7.4	8.7	0.41	152	77.6 ± 6.3

Model	PTC-MR				IMDB-B			
	Pre	Train	Run	Val	Pre	Train	Run	Val
SGCN	0.1	0.29	102	63.6 ± 9.7	0.4	0.33	116	74.2 ± 3.4
SIGN	0.2	0.30	105	64.5 ± 5.8	0.5	0.36	126	74.5 ± 5.4
SE2P-C2	1.7	0.28	101	65.1 ± 7.3	3.8	0.38	137	75.2 ± 2.9

Model	IMDB-M				COLLAB			
	Pre	Train	Run	Val	Pre	Train	Run	Val
SGCN	0.5	0.37	130	51.4 ± 2.9	4.8	0.46	166	80.8 ± 1.7
SIGN	0.7	0.38	133	51.6 ± 3.7	6.8	0.71	255	82.3 ± 1.8
SE2P-C2	4.0	0.37	133	52.3 ± 3.5	224.2	0.72	476	83.3 ± 2.1

graph in the training phase to be fitted into the memory.¹³ In contrast, SE2P-C2 *efficiently* outperforms the best-performing baseline with a 0.7% improvement. One might wonder why SE2P-C4 does not outperform all other configurations despite involving more training steps and feature extraction. We hypothesize that the main issue could be our adopted cascading approach for hyperparameter tuning, which may have led to suboptimal optimization for this configuration compared to the others.

We further compare the runtime efficiency of SE2P configurations with GCN, GIN, DropGCN, and DropGIN in Table 5. The preprocessing time of SE2P for most datasets is relatively short, ranging from a minimum of half a second for MUTAG to a maximum of 4 minutes for COLLAB.¹⁴ Across all datasets, SE2P-C1 and SE2P-C2 emerged as faster models for training time and total runtime (including preprocessing and training time over all epochs) than the baselines. The speedup for total runtime ranges from 3.19× (in PROTEINS) to 7.90× (in PTC-MR) for SE2P-C1, and from 2.16× (in PROTEINS) to 6.02× (in PTC-MR) for SE2P-C2. SE2P-C3 achieves a runtime comparable to the baselines (except for COLLAB due to a

¹³Although we encountered out-of-memory issues for DropGNN on the COLLAB dataset due to the large number of graphs and perturbations, we can avoid this issue by decreasing the batch size (e.g., from 32 to 6 in DropGCN on our tested server) to run these models on this dataset. When tested on such small batch sizes, we noticed the suboptimal performance of DropGNN. So, we reported OOM results to emphasize the computational bottleneck rather than expressiveness concerns.

¹⁴The reported preprocessing time is the time taken to preprocess the dataset and load it into memory. The process may require additional time if there is a need to write the preprocessed datasets to disk.

large number of graphs) while improving generalizability. SE2P-C4 is the slowest model, as it involves more training time than the others. In general, if scalability of 3-6× is desired while keeping generalizability comparable, SE2P-C2 is the best option. If one aims to maintain scalability comparable to the baselines while improving generalizability up to 1.5%, SE2P-C3 is recommended.

Our SE2P methods on the OGB datasets demonstrate promising results, as shown in Table 6. In OGBG-MOLHIV, SE2P-C2 achieves comparable results to the baselines while offering a speedup of roughly 30%. SE2P-C3 outperforms baseline methods but at the expense of longer training times. DropGCN, DropGIN, and SE2P-C4 encountered out-of-memory issues, primarily due to the large number of graphs in this dataset (48, 127 graphs). These issues arose from the application of message-passing over many graph perturbations (for DropGCN and DropGIN) or feature transformation over diffusion sets of all perturbations of a graph (for SE2P-C4) during the training phase. For OGBG-MOLTOX, all methods utilizing node-dropout perturbations (except SE2P-C1, which lacks sufficient non-linearity and expressivity) outperform the two baselines without graph perturbations. For comparable performance and faster runtime, SE2P-C2 is preferred. It demonstrates roughly a 30% speed improvement over the fastest baseline (GIN) and a 130% speed improvement over the slowest baseline (DropGCN). If higher generalization is sought, SE2P-C3 and SE2P-C4 are recommended at the expense of reduced scalability.

Ablation study. Our ablation studies intend to assess the effectiveness of perturbations and aggregator functions of COMBINE and MERGE on the generalizability of SE2P-C2.¹⁵ By excluding the generation of perturbations and MERGE from SE2P-C2, we obtain a variant SIGN [19]. For this model, we keep COMBINE and POOL the same as SE2P-C2. From SIGN, we further remove COMBINE, thus only applying one diffusion matrix (i.e., the L th power of adjacency matrix). The resulting model is SGCN [54] with the same POOL function of SE2P-C2. Note that these two SIGN and SGCN variants not only allow us to conduct our ablation studies but also enable us to assess the extent of generalizability provided by the higher expressiveness of our SE2P models.

Table 7 reports the results of our ablation studies. For all datasets, SE2P-C2 with node-dropout perturbation outperforms both SGCN and SIGN, which do not have any perturbations. This suggests that the expressive power offered by perturbations can lead to improved generalizability. Recall that the expressive power of SGCN and SIGN is bound by the 1-WL. However, we can surpass this limitation by generating perturbations and achieving better results on benchmark datasets. The runtime of SE2P-C2 is comparable with those of SGCN and SIGN across all datasets except for COLLAB, for which our model has a longer preprocessing time. This is due to both the large number of graphs and high average-degree graphs, which dictate a larger number of required perturbations for each graph.

6 CONCLUSION AND FUTURE WORK

We introduced SE2P, a flexible framework with four configuration classes that balance scalability and generalizability. SE2P leverages graph perturbations and feature diffusion in the preprocessing stage

¹⁵We have selected SE2P-C2 as our subject of ablation studies due to its both competitive generalizability and improved scalability/runtime, compared to baselines.

and offers choices between learnable and non-learnable aggregator functions to achieve the desirable scalability-expressiveness balance. Our experiments on an extensive set of benchmarks validate the effectiveness of SE2P, demonstrating significant speed improvements and enhanced generalizability depending on the selected configuration. Future directions include exploring other graph perturbation policies beyond node dropout, providing theoretical analyses of graph perturbations through the lens of matrix perturbation theory, and developing adaptive and learnable methods for selecting the number of graph perturbations.

REFERENCES

- [1] Siddhant Arora. 2020. A survey on graph neural networks for knowledge graph completion. *arXiv preprint arXiv:2007.12374* (2020).
- [2] James Atwood and Don Towsley. 2016. Diffusion-convolutional neural networks. *Advances in neural information processing systems* 29 (2016).
- [3] Waiss Azizian and Marc Lelarge. 2020. Expressive power of invariant and equivariant graph neural networks. *arXiv preprint arXiv:2006.15646* (2020).
- [4] Pablo Barceló, Floris Geerts, Juan Reutter, and Maksimilian Ryschkov. 2021. Graph neural networks with local graph parameters. *Advances in Neural Information Processing Systems* 34 (2021), 25280–25293.
- [5] Beatrice Bevilacqua, Fabrizio Frasca, Derek Lim, Balasubramaniam Srinivasan, Chen Cai, Gopinath Balamurugan, Michael M Bronstein, and Haggai Maron. 2021. Equivariant subgraph aggregation networks. *arXiv preprint arXiv:2110.02910* (2021).
- [6] Karsten M Borgwardt, Cheng Soon Ong, Stefan Schönauer, SVN Vishwanathan, Alex J Smola, and Hans-Peter Kriegel. 2005. Protein function prediction via graph kernels. *Bioinformatics* 21, suppl_1 (2005), i47–i56.
- [7] Giorgos Bouritsas, Fabrizio Frasca, Stefanos Zafeiriou, and Michael M Bronstein. 2022. Improving graph neural network expressivity via subgraph isomorphism counting. *IEEE Transactions on Pattern Analysis and Machine Intelligence* 45, 1 (2022), 657–668.
- [8] David Buterez, Jon Paul Janet, Steven J Kiddle, Dino Oglic, and Pietro Liò. 2022. Graph neural networks with adaptive readouts. *Advances in Neural Information Processing Systems* 35 (2022), 19746–19758.
- [9] Cătălina Cangea, Petar Veličković, Nikola Jovanović, Thomas Kipf, and Pietro Liò. 2018. Towards sparse hierarchical graph classifiers. *arXiv preprint arXiv:1811.01287* (2018).
- [10] Jie Chen, Tengfei Ma, and Cao Xiao. 2018. Fastgcn: fast learning with graph convolutional networks via importance sampling. *arXiv preprint arXiv:1801.10247* (2018).
- [11] Jianfei Chen and Jun Zhu. 2018. Stochastic training of graph convolutional networks. (2018).
- [12] Wei-Lin Chiang, Xuanqing Liu, Si Si, Yang Li, Samy Bengio, and Cho-Jui Hsieh. 2019. Cluster-gcn: An efficient algorithm for training deep and large graph convolutional networks. In *Proceedings of the 25th ACM SIGKDD international conference on knowledge discovery & data mining*. 257–266.
- [13] Leonardo Cotta, Christopher Morris, and Bruno Ribeiro. 2021. Reconstruction for powerful graph representations. *Advances in Neural Information Processing Systems* 34 (2021), 1713–1726.
- [14] Asim Kumar Debnath, Rosa L Lopez de Compadre, Gargi Debnath, Alan J Shusterman, and Corwin Hansch. 1991. Structure-activity relationship of mutagenic aromatic and heteroaromatic nitro compounds. correlation with molecular orbital energies and hydrophobicity. *Journal of medicinal chemistry* 34, 2 (1991), 786–797.
- [15] Paul D Dobson and Andrew J Doig. 2003. Distinguishing enzyme structures from non-enzymes without alignments. *Journal of molecular biology* 330, 4 (2003), 771–783.
- [16] Vijay Prakash Dwivedi, Anh Tuan Luu, Thomas Laurent, Yoshua Bengio, and Xavier Bresson. 2022. Graph Neural Networks with Learnable Structural and Positional Representations. In *International Conference on Learning Representations*.
- [17] Wenzheng Feng, Jie Zhang, Yuxiao Dong, Yu Han, Huanbo Luan, Qian Xu, Qiang Yang, Evgeny Kharlamov, and Jie Tang. 2020. Graph random neural networks for semi-supervised learning on graphs. *Advances in neural information processing systems* 33 (2020), 22092–22103.
- [18] Fabrizio Frasca, Beatrice Bevilacqua, Michael Bronstein, and Haggai Maron. 2022. Understanding and extending subgraph gnns by rethinking their symmetries. *Advances in Neural Information Processing Systems* 35 (2022), 31376–31390.
- [19] Fabrizio Frasca, Emanuele Rossi, Davide Eynard, Benjamin Chamberlain, Michael Bronstein, and Federico Monti. 2020. SIGN: Scalable Inception Graph Neural Networks. In *ICML 2020 Workshop on Graph Representation Learning and Beyond*.
- [20] Hongyang Gao and Shuiwang Ji. 2019. Graph u-nets. In *international conference on machine learning*. PMLR, 2083–2092.
- [21] Wenhao Gao, Sai Pooja Mahajan, Jeremias Sulam, and Jeffrey J Gray. 2020. Deep learning in protein structural modeling and design. *Patterns* 1, 9 (2020).
- [22] Justin Gilmer, Samuel S Schoenholz, Patrick F Riley, Oriol Vinyals, and George E Dahl. 2017. Neural message passing for quantum chemistry. In *International conference on machine learning*. PMLR, 1263–1272.
- [23] Will Hamilton, Zhitao Ying, and Jure Leskovec. 2017. Inductive representation learning on large graphs. *Advances in neural information processing systems* 30 (2017).
- [24] William L Hamilton. 2020. *Graph representation learning*. Morgan & Claypool Publishers.
- [25] Weihua Hu, Matthias Fey, Marinka Zitnik, Yuxiao Dong, Hongyu Ren, Bowen Liu, Michele Catasta, and Jure Leskovec. 2020. Open graph benchmark: Datasets for machine learning on graphs. *Advances in neural information processing systems* 33 (2020), 22118–22133.
- [26] Wenbing Huang, Tong Zhang, Yu Rong, and Junzhou Huang. 2018. Adaptive sampling towards fast graph representation learning. *Advances in neural information processing systems* 31 (2018).
- [27] Yinan Huang, Xingang Peng, Jianzhu Ma, and Muhan Zhang. 2022. Boosting the Cycle Counting Power of Graph Neural Networks with l^2 -GNNs. *arXiv preprint arXiv:2210.13978* (2022).
- [28] Thomas N Kipf and Max Welling. 2016. Semi-supervised classification with graph convolutional networks. *arXiv preprint arXiv:1609.02907* (2016).
- [29] Boris Knyazev, Graham W Taylor, and Mohamed Amer. 2019. Understanding attention and generalization in graph neural networks. *Advances in neural information processing systems* 32 (2019).
- [30] Junhyun Lee, Inyeop Lee, and Jaewoo Kang. 2019. Self-attention graph pooling. In *International conference on machine learning*. PMLR, 3734–3743.
- [31] Juho Lee, Yoonho Lee, Jungtaek Kim, Adam Kosiorek, Seungjin Choi, and Yee Whye Teh. 2019. Set transformer: A framework for attention-based permutation-invariant neural networks. In *International conference on machine learning*. PMLR, 3744–3753.
- [32] AA Leman and Boris Weisfeiler. 1968. A reduction of a graph to a canonical form and an algebra arising during this reduction. *Nauchno-Technicheskaya Informatsiya* 2, 9 (1968), 12–16.
- [33] Pan Li, Yanbang Wang, Hongwei Wang, and Jure Leskovec. 2020. Distance encoding: Design provably more powerful neural networks for graph representation learning. *Advances in Neural Information Processing Systems* 33 (2020), 4465–4478.
- [34] Yujia Li, Chenjie Gu, Thomas Dullien, Oriol Vinyals, and Pushmeet Kohli. 2019. Graph matching networks for learning the similarity of graph structured objects. In *International conference on machine learning*. PMLR, 3835–3845.
- [35] Yujia Li, Daniel Tarlow, Marc Brockschmidt, and Richard Zemel. 2015. Gated graph sequence neural networks. *arXiv preprint arXiv:1511.05493* (2015).
- [36] Paul Louis, Shweta Ann Jacob, and Amirali Salehi-Abari. 2022. Sampling enclosing subgraphs for link prediction. In *Proceedings of the 31st ACM International Conference on Information & Knowledge Management*. 4269–4273.
- [37] Paul Louis, Shweta Ann Jacob, and Amirali Salehi-Abari. 2023. Simplifying subgraph representation learning for scalable link prediction. *arXiv preprint arXiv:2301.12562* (2023).
- [38] Haggai Maron, Heli Ben-Hamu, Hadar Serviansky, and Yaron Lipman. 2019. Provably powerful graph networks. *Advances in neural information processing systems* 32 (2019).
- [39] Haggai Maron, Heli Ben-Hamu, Nadav Shamir, and Yaron Lipman. 2018. Invariant and equivariant graph networks. *arXiv preprint arXiv:1812.09902* (2018).
- [40] Christopher Morris, Kristian Kersting, and Petra Mutzel. 2017. Globalized weisfeiler-lehman graph kernels: Global-local feature maps of graphs. In *2017 IEEE International Conference on Data Mining (ICDM)*. IEEE, 327–336.
- [41] Christopher Morris, Nils M. Kriege, Franka Bause, Kristian Kersting, Petra Mutzel, and Marion Neumann. 2020. TUDataset: A collection of benchmark datasets for learning with graphs. In *ICML 2020 Workshop on Graph Representation Learning and Beyond (GRL+ 2020)*.
- [42] Christopher Morris, Gaurav Rattan, Sandra Kiefer, and Siamak Ravanbakhsh. 2022. Speqnets: Sparsity-aware permutation-equivariant graph networks. In *International Conference on Machine Learning*. PMLR, 16017–16042.
- [43] Christopher Morris, Gaurav Rattan, and Petra Mutzel. 2020. Weisfeiler and Leman go sparse: Towards scalable higher-order graph embeddings. *Advances in Neural Information Processing Systems* 33 (2020), 21824–21840.
- [44] Christopher Morris, Martin Ritzert, Matthias Fey, William L Hamilton, Jan Eric Lenssen, Gaurav Rattan, and Martin Grohe. 2019. Weisfeiler and leman go neural: Higher-order graph neural networks. In *Proceedings of the AAAI conference on artificial intelligence*, Vol. 33. 4602–4609.
- [45] Alireza A Namanloo, Julie Thorpe, and Amirali Salehi-Abari. 2022. Improving Peer Assessment with Graph Neural Networks. *International Educational Data Mining Society* (2022).

- [46] Mathias Niepert, Mohamed Ahmed, and Konstantin Kutzkov. 2016. Learning convolutional neural networks for graphs. In *International conference on machine learning*. PMLR, 2014–2023.
- [47] Pál András Papp, Karolis Martinkus, Lukas Faber, and Roger Wattenhofer. 2021. DropGNN: Random dropouts increase the expressiveness of graph neural networks. *Advances in Neural Information Processing Systems* 34 (2021), 21997–22009.
- [48] Pál András Papp and Roger Wattenhofer. 2022. A theoretical comparison of graph neural network extensions. In *International Conference on Machine Learning*. PMLR, 17323–17345.
- [49] Yu Rong, Wenbing Huang, Tingyang Xu, and Junzhou Huang. 2020. DropEdge: Towards Deep Graph Convolutional Networks on Node Classification. In *International Conference on Learning Representations*.
- [50] Nino Shervashidze, Pascal Schweitzer, Erik Jan Van Leeuwen, Kurt Mehlhorn, and Karsten M Borgwardt. 2011. Weisfeiler-lehman graph kernels. *Journal of Machine Learning Research* 12, 9 (2011).
- [51] Zhihao Shi, Xize Liang, and Jie Wang. 2023. LMC: Fast training of GNNs via subgraph sampling with provable convergence. *arXiv preprint arXiv:2302.00924* (2023).
- [52] Hannu Toivonen, Ashwin Srinivasan, Ross D King, Stefan Kramer, and Christoph Helma. 2003. Statistical evaluation of the predictive toxicology challenge 2000–2001. *Bioinformatics* 19, 10 (2003), 1183–1193.
- [53] Ameya Velingker, Ali Kemal Sinop, Ira Ktena, Petar Veličković, and Sreenivas Gollapudi. 2022. Affinity-aware graph networks. *arXiv preprint arXiv:2206.11941* (2022).
- [54] Felix Wu, Amauri Souza, Tianyi Zhang, Christopher Fifty, Tao Yu, and Kilian Weinberger. 2019. Simplifying graph convolutional networks. In *International conference on machine learning*. PMLR, 6861–6871.
- [55] Shiwen Wu, Fei Sun, Wentao Zhang, Xu Xie, and Bin Cui. 2022. Graph neural networks in recommender systems: a survey. *Comput. Surveys* 55, 5 (2022), 1–37.
- [56] Keyulu Xu, Weihua Hu, Jure Leskovec, and Stefanie Jegelka. 2019. How Powerful are Graph Neural Networks?. In *International Conference on Learning Representations*.
- [57] Keyulu Xu, Chengtao Li, Yonglong Tian, Tomohiro Sonobe, Ken-ichi Kawarabayashi, and Stefanie Jegelka. 2018. Representation learning on graphs with jumping knowledge networks. In *International conference on machine learning*. PMLR, 5453–5462.
- [58] Pinar Yanardag and SVN Vishwanathan. 2015. Deep graph kernels. In *Proceedings of the 21th ACM SIGKDD international conference on knowledge discovery and data mining*. 1365–1374.
- [59] Rex Ying, Ruining He, Kaifeng Chen, Pong Eksombatchai, William L Hamilton, and Jure Leskovec. 2018. Graph convolutional neural networks for web-scale recommender systems. In *Proceedings of the 24th ACM SIGKDD international conference on knowledge discovery & data mining*. 974–983.
- [60] Zhitao Ying, Jiaxuan You, Christopher Morris, Xiang Ren, Will Hamilton, and Jure Leskovec. 2018. Hierarchical graph representation learning with differentiable pooling. *Advances in neural information processing systems* 31 (2018).
- [61] Jiaxuan You, Jonathan M Gomes-Selman, Rex Ying, and Jure Leskovec. 2021. Identity-aware graph neural networks. In *Proceedings of the AAAI conference on artificial intelligence*, Vol. 35. 10737–10745.
- [62] Manzil Zaheer, Satwik Kottur, Siamak Ravanbakhsh, Barnabas Poczos, Russ R Salakhutdinov, and Alexander J Smola. 2017. Deep sets. *Advances in neural information processing systems* 30 (2017).
- [63] Hanqing Zeng, Hongkuan Zhou, Ajitesh Srivastava, Rajgopal Kannan, and Viktor Prasanna. 2019. Graphsaint: Graph sampling based inductive learning method. *arXiv preprint arXiv:1907.04931* (2019).
- [64] Muhan Zhang, Zhicheng Cui, Marion Neumann, and Yixin Chen. 2018. An end-to-end deep learning architecture for graph classification. In *Proceedings of the AAAI conference on artificial intelligence*, Vol. 32.
- [65] Muhan Zhang and Pan Li. 2021. Nested graph neural networks. *Advances in Neural Information Processing Systems* 34 (2021), 15734–15747.
- [66] Muhan Zhang, Pan Li, Yinglong Xia, Kai Wang, and Long Jin. 2021. Labeling trick: A theory of using graph neural networks for multi-node representation learning. *Advances in Neural Information Processing Systems* 34 (2021), 9061–9073.
- [67] Wentao Zhang, Zeang Sheng, Mingyu Yang, Yang Li, Yu Shen, Zhi Yang, and Bin Cui. 2022. NAFS: A Simple yet Tough-to-beat Baseline for Graph Representation Learning. In *International Conference on Machine Learning*. PMLR, 26467–26483.
- [68] Yongqi Zhang and Quanming Yao. 2022. Knowledge graph reasoning with relational digraph. In *Proceedings of the ACM web conference 2022*. 912–924.
- [69] Lingxiao Zhao, Wei Jin, Leman Akoglu, and Neil Shah. 2022. From Stars to Subgraphs: Uplifting Any GNN with Local Structure Awareness. In *International Conference on Learning Representations*.
- [70] Difan Zou, Ziniu Hu, Yewen Wang, Song Jiang, Yizhou Sun, and Quanquan Gu. 2019. Layer-dependent importance sampling for training deep and large graph convolutional networks. *Advances in neural information processing systems* 32 (2019).

A HYPER-PARAMETERS

The hyperparameters of our models (C1–C4) are shared and nested, with each more expressive configuration introducing new hyperparameters while retaining those of the less expressive model. This nested structure allows us to adopt a cascading approach for hyperparameter tuning from the SE2P-C1 to the SE2P-C4, which helps in reducing our search space. Beginning with the least expressive configuration SE2P-C1, we optimized its hyperparameters and then fixed them for use in the SE2P-C2, tuning only the newly introduced hyperparameters for this configuration. We repeated this process, fixing the optimized hyperparameters of each configuration for the subsequent one (SE2P-C3 and SE2P-C4), and applied the hyperparameter tuning only on the new hyperparameters. For instance, when moving from SE2P-C2 to SE2P-C3, we search for two new hyperparameters: the number of inner and outer MLP layers in the DeepSet’s MERGE function of SE2P-C3, while keeping the other hyperparameters the same as in SE2P-C2. While this strategy reduces the search space, it may compromise the optimal performance of the more expressive configurations, as they might be tuned to suboptimal hyperparameters. Table 8 reports our tuned hyperparameters for all four instances and datasets.

B NUMBER OF PARAMETERS

We derive equations for calculating the number of learnable parameters for each examined configuration of SE2P. We first compute the size of each learning component used in any of our configurations, then drive the size of configurations based on which components are used in them. We denote L as the number of virtual layers for the diffusion step. The model size of M is denoted by $|M|$ in our analyses below.

All of our models have final MLP_f with N_f hidden layers for classification; we compute its number of parameters as a function of its input size h_0 . Assuming C is the number of classes, this MLP has $\sum_{k=0}^{N_f-1} h_k h_{k+1} + h_{N_f} c$ parameters, where h_k is the dimensionality of the k^{th} hidden layer. For this MLP, we reduce the dimensionality of each hidden layer by a factor of 0.5, i.e., $h_i = \frac{h_{i-1}}{2}$. Thus, $h_k = \frac{h_0}{2^k}$. In all experiments in this paper, we set $N_f = 1$, so the number of parameters as a function of its input size h_0 is calculated by:

$$|MLP_f(h_0)| = \frac{h_0}{2}(h_0 + C). \quad (12)$$

Three configurations have MLP_p as part of their learnable pooling functions. MLP_p has N_p hidden layers, each having fixed hidden dimensionality h ; we compute its number of parameters as a function of its input size h_0 . Assuming h is also its output dimensionality, this MLP has

$$|MLP_p(h_0)| = h_0 h + N_p h^2. \quad (13)$$

DeepSet has been employed as a learning component for either COMBINE or MERGE functions in two configurations SE2P-C3 and SE2P-C4. Assuming its inner and outer MLPs have N_{inn} and N_{out} hidden layers with hidden dimensionality h , we compute its number of parameters as a function of its input size h_0 :

$$\begin{aligned} |DS(h_0)| &= h_0 h + N_{inn} h^2 + (N_{out} + 1) h^2 \\ &= h_0 h + (N_{inn} + N_{out} + 1) h^2. \end{aligned} \quad (14)$$

From now on, we define N_{inn}^{fn} and N_{out}^{fn} as the number of hidden layers in the inner and outer MLPs of the Deepset DS^{fn} , where fn specifies either the MERGE function or the COMBINE function, denoted by *mer* and *com*, respectively.

The learnable parameters of SE2P-C1 are only from an MLP with one hidden layer for final classification and input size of $(L + 1)d$. So the number of learnable parameters are:

$$\begin{aligned} |SE2P-C1| &= |MLP_f((L + 1)d)| \\ &= \frac{(L + 1)d}{2}((L + 1)d + C) \end{aligned} \quad (15)$$

SE2P-C2 has two MLPs, one for pooling MLP_p with input size $(L + 1)d$ and the other one for the final classification MLP_f with h input size. So its number of parameters is:

$$\begin{aligned} |SE2P-C2| &= |MLP_p((L + 1)d)| + |MLP_f(h)| \\ &= (L + 1)dh + N_p h^2 + \frac{h}{2}(h + C) \\ &= (L + 1)dh + (N_p + \frac{1}{2})h^2 + \frac{Ch}{2} \\ &= (Ld + d + C/2)h + (N_p + \frac{1}{2})h^2 \end{aligned} \quad (16)$$

SE2P-C3 has DS^{mer} with input size of $(L + 1)d$, MLP_p with input size h , MLP_f with input size of h . So its size is given by:

$$\begin{aligned} |SE2P-C3| &= |DS^{mer}((L + 1)d)| + |MLP_p(h)| + |MLP_f(h)| \\ &= (L + 1)dh + (N_{inn}^{mer} + N_{out}^{mer} + 1)h^2 \\ &\quad + (N_p + 1)h^2 + \frac{h}{2}(h + C) \\ &= (Ld + d + C/2)h + (N_{inn}^{mer} + N_{out}^{mer} + N_p + \frac{5}{2})h^2 \end{aligned} \quad (17)$$

SE2P-C4 has DS^{com} with input size d , DS^{mer} with input size h , MLP_p with input size h , and MLP_f with input size of h . So, its number of parameters are:

$$\begin{aligned} |SE2P-C4| &= |DS^{com}(d)| + |DS^{mer}(h)| + |MLP_p(h)| + |MLP_f(h)| \\ &= dh + (N_{inn}^{com} + N_{out}^{com} + 1)h^2 + (N_{inn}^{mer} + N_{out}^{mer} + 2)h^2 \\ &\quad + (N_p + 1)h^2 + \frac{h}{2}(h + C) \\ &= (N_{inn}^{mer} + N_{out}^{mer} + N_{inn}^{com} + N_{out}^{com} + N_p + \frac{9}{2})h^2 \\ &\quad + (\frac{C}{2} + d)h. \end{aligned} \quad (18)$$

Table 8: Selected hyperparameters for each dataset. L denotes the number of virtual layers for the diffusion step. N_f is the number of hidden layers in the final MLP. N_p is the number of hidden layers in the POOL function. N_{inn}^{mer} and N_{out}^{mer} are the number of hidden layers in the inner and outer MLP of the Deepset in the MERGE function. N_{inn}^{com} and N_{out}^{com} are the number of hidden layers in the inner and outer MLP of the Deepset in the COMBINE function. h is the hidden dimensionality of all MLPs except the final MLP. The MLPs with zero hidden layers are single non-linear transformations.

Dataset	SE2P-C4										
	SE2P-C3										
	SE2P-C2										
	SE2P-C1										
	Batchsize	Dropout	L	N_f	N_p	h	N_{inn}^{mer}	N_{out}^{mer}	N_{inn}^{com}	N_{out}^{com}	
MUTAG	64	0.5	3	1	3	32	1	1	1	2	
PROTEINS	64	0.5	3	1	2	16	2	2	0	3	
PTC-MR	32	0.0	3	1	1	32	0	0	0	0	
IMDB-B	32	0.5	2	1	3	32	0	0	3	2	
IMDB-M	32	0.5	2	1	3	32	2	2	0	1	
COLLAB	32	0.5	2	1	2	32	0	0	0	0	
OGBG-MOLHIV	256	0.0	3	1	2	32	0	1	N/A	N/A	
OGBG-MOLTOX	64	0.0	3	1	3	64	1	1	0	0	

Table 9: Number of learnable parameters.

Model	MUTAG	PROTEINS	PTC-MR	IMDB-B	IMDB-M	COLLAB	OGBG-MOLHIV	OGBG-MOLTOX
GIN	2440	2368	2656	35284	35614	63955	31054	34024
GCN	3960	1152	4368	18132	18462	80595	13902	16872
DropGIN	2440	2368	2656	35284	35614	N/A	N/A	34024
DropGCN	3960	1152	3744	18132	18462	N/A	N/A	16872
SE2P-C1	464	104	3080	21838	21942	1093719	721	930
SE2P-C2	4914	1002	4210	10642	10659	50147	4033	5340
SE2P-C3	9394	2826	6450	12882	17379	52387	8513	34988
SE2P-C4	14322	4202	6866	16306	16323	23139	N/A	41836